

Water absorption and chloride diffusivity of concrete under the coupling effect of uniaxial compressive load and freeze-thaw cycles

Yanru Wang ^{a,b}, Yubin Cao ^{a,b}, Peng Zhang ^{a,*}, Yuwei Ma ^{d,b,*}, Tiejun Zhao ^a, Hao Wang ^b,

Zuhua Zhang ^{b,c}

^a College of Civil Engineering, Qingdao University of Technology, Qingdao, 266033, PR China

^b Centre for Future Materials, University of Southern Queensland, Toowoomba, QLD 4350, Australia

^c Key Laboratory for Green & Advanced Civil Engineering Materials and Application Technology of Hunan Province, College of Civil Engineering, Hunan University, Changsha 410082, PR China

^d Guangzhou University - Tamkang University Joint Research Center for Engineering Structure Disaster Prevention and Control, Guangzhou University, Guangzhou 510006, China

E-mails of corresponding authors: peng.zhang@qut.edu.cn; yuwei.ma@hotmail.com

Abstract:

In cold coastal area, the destruction mechanism of reinforced concrete structures is mainly governed by a combination of factors such as self-loading, freeze-thaw and chloride erosion. In this study, ordinary cube concretes (C30 and C50, while $w/c = 0.53$ and 0.35 respectively) underwent a coupling effect of pressure load with stress ratio of 0, 0.3 and 0.5 and freeze-thaw cycles, following by capillary water absorption test and chloride penetration test. Concrete samples with $0.3f_c$ showed the best water and chloride penetration resistance under the coupling effect, followed by samples with $0.5f_c$ and $0f_c$, which is consistent with the conclusion that under load only. Water and chloride ions penetration increased sharply when freeze-thaw cycles was over 100 times, which is different with samples without load. Outside part of concrete showed higher permeability and chloride content than inside part. MIP results confirmed that stress played an important role in the water absorption and chloride penetration

24 of concrete under the coupling effect. These results provide important new insights into the
25 permeability of concrete under a coupling effect. The applied load performed a more important
26 role on the service life prediction of concrete structure.

27 **Keywords:** Coupling effect; Freeze-thaw; Load; Capillary Water; Chloride

28 **1. Introduction**

29 Reinforced concrete is widely used in construction around the world, mainly due to its low cost,
30 high mechanical strength and stability [1]. However, deterioration of concrete structures have
31 been reported both in literature and in practice, particularly when concrete is served in harsh
32 environment, leading to decline of concrete strength and corrosion of reinforced rebar [2, 3]. It
33 is thus accepted that the durability and service life of concrete structures should be considered
34 in future construction design. In general, the durability and service life of concrete are mainly
35 governed by a series of environmental factors, e.g. freeze-thaw, carbonation, sulphate attack
36 and chloride penetration etc. [4]. In practice, most concrete structures are exposed to coupling
37 environmental actions. In cold coastal area, such as the north area of China, freeze-thaw and
38 chloride penetration are the main deteriorating processes for reinforced concrete structures [5].
39 Chloride ions were detrimental ions affecting the service life of reinforced concretes. The
40 presence of free chloride ions in environments could penetrate concrete and result in corrosion
41 of reinforced bar. According to Yang et al. [6], the main transport processes in concrete included
42 capillary absorption, diffusion, permeation, and convection. As for capillary force or gradient
43 of capillary potential, the water is absorbed into concrete through pores, while diffusion

44 happened mainly because of a concentration gradient [7, 8]. Penetration is a transport process
45 of water and air into concrete, which is caused by gravity or pressure gradient; and convection
46 is the process happened in solution such as the transport of chloride or sulphate ions into
47 concrete [9, 10]. In real construction, it is usually more than one process occurring at the same
48 time, and each of these mechanisms are influenced by internal microstructure of concrete and
49 external environment.

50 The pore structure of concrete has a crucial influence on the process of chloride penetration;
51 and water is the main transfer medium [11-18]. According to Mehta [19] and Chen [20], with
52 the decrease of the pore aperture size (r), the water penetration depth decreases firstly ($r \geq$
53 $1000 \sim 10000$ nm) and then increase ($100 \text{ nm} \leq r \leq 1000$ nm), and finally decreased again (r
54 ≤ 100 nm). In addition, the aperture size smaller, the freezing point lower, and the freezing
55 rate in concrete pore lower. Finally, the damage caused by the expansion of pore water lower
56 [21].

57 Hence, study on the migration of water in concrete is important. The frozen of pore solution
58 caused by freeze-thaw process created internal pressure in pores and led to damage of concrete.
59 The respective effect of chloride penetration and freeze-thaw cycles on the durability of
60 concrete has been extensively investigated in previous studies [22-25]. It was reported that the
61 penetration of chloride into concrete was related to the pore structure and cracks in concrete
62 [23, 26-28]. Costa and Appleton [29] presented the results of an experimental study of the two
63 concrete mixes (water/cement ratio = 0.3 and 0.5) in four different marine exposure conditions

64 (spray zone, tidal zone, atmospheric zone and dockyard zone) for five years. The results
65 showed that the chloride penetration of concrete ($w/c = 0.5$) in tidal zone was highest. The
66 authors speculated that the chloride penetration strongly dependent on both the concrete
67 mixture and the exposure conditions. Collepari et al. [30] did chloride diffusion test of
68 Portland cement at different experimental temperature, i.e. 10°C, 20°C and 40°C and found
69 that the diffusion coefficients of chloride ion into Portland cement pastes increased with the
70 increase of temperature.

71 Freeze-thaw cycles accelerate the damage evolution of concrete and reduce the service life of
72 concrete structures. Cai and Liu [31] observed the change of electrical conductivity of concrete
73 exposed to a refrigerator (temperature varied from 0 °C to -20 °C) and concluded that the frozen
74 of pore solution between 0 °C to -10 °C determined the durability of concrete. Molero et al.
75 [32] applied ultrasonic imaging to evaluation the degradation process of normal concrete and
76 air-contained concrete exposed to freeze-thaw cycles and found that the later showed better
77 frost resistance than the former.

78 Studies also suggested that the main factor to improve the freeze-thaw resistance relied on the
79 compact of concrete . explained that mix design of concrete could influence its compaction
80 energy, which then significantly affected the freeze-thaw durability of Portland cement
81 concrete and, to a less extent, reduced compressive strength and split strength and increased
82 permeability.

83 Apart from single environmental factor, coupling effect of two or more environmental factors
84 is considered recently. Zhang et al. [23] used Neutron radiography to study the influence of
85 freeze-thaw cycles on capillary absorption and chloride penetration concrete. They found that
86 the freeze-thaw cycles increased the rate of water absorption and chloride penetration. Yang et
87 al. [6] studied water transport in concrete after freeze-thaw cycling. They found that both the
88 total water absorption and the initial water absorption coefficient increased after 500 freeze-
89 thaw cycles due to the frost induced cracks.

90 In practise, most reinforced concrete structures are used under load. The consideration of load
91 combined with environmental actions could provide more practical and reliable results when
92 evaluate the durability and service life of concrete. Sun and Lu [33] demonstrated that the
93 permeability of concrete increased under 60% ultimate load during coupling effect of axially
94 distributed load and carbonization. Bao and Wang [34] found that with the increase of
95 compression stress load, the chloride content decreased firstly and then increased after a critical
96 stress level. Sun et al. [35] found that the stress ratio was an important influencing factor on
97 performance of concrete; concrete subjected to higher stress ratio, presented greater frost
98 damage.

99 The previous study most focus on mechanical load and one environmental load (i.e. load +
100 carbonization/freeze-thaw/chloride penetration et al.) or two environmental loads (i.e. freeze-
101 thaw + carbonization/chloride penetration). This paper studied the coupling effect of
102 mechanical load and two environmental loads, i.e. mechanical load + freeze-thaw + chloride

103 penetration, which could provide a new insight on the prediction of reinforcement concrete
104 structure.

105 **2. Materials and Methods**

106 **2.1 Materials**

107 Portland cement Type I was used as the raw material for the concrete. The chemical
108 composition of cement measured by X fluorescent spectrometry (XRF) was shown in Table 1.
109 Its specific surface area was 350~370 m²/kg. The average particle size was around 27 μm; and
110 the particles size less than 3 μm and 3-30 μm accounted for about 6.7% and 70%, respectively,
111 meeting the requirements for optimum cement performance proposed by Tsivilis et al. [36].
112 River sand with a Fineness modulus of 2.7 and granite gravel with a distribution diameter
113 between 5 mm and 20 mm (obtained from Qingdao, China) were used as fine aggregate and
114 coarse aggregate, respectively. For C50 concrete, PCA®-I polycarboxylic acid high
115 performance water reducing agent (produced by Subute New Materials Co., Ltd.) were used to
116 obtain the slump and fluidity in line with real construction requirements.

117 **2.2 Sample preparation**

118 Concrete was prepared with by different strength category, i.e. C30 and C50, according to
119 JGJ/55-2011 [36]. Table 2 shows the mixture composition of each concrete. The water to
120 cement ratio for C30 and C50 was 0.53 and 0.35, respectively. Firstly, mixing solid materials
121 at horizontal concrete mixer for 1 minute, then add water (with superplastizer) into mixture

122 stirring for another 3 minutes. After mixing, fresh concrete was cast into 100 mm ×100 mm ×
123 100 mm cube mould. After 1 day curing at room temperature, all concrete specimens were
124 demoulded and cured in a curing room (relative humidity of 95% and temperature of 20 ± 2 °C)
125 for 23 days. Before loading and freeze-thaw test, concrete samples were immersed into water
126 for another 4 days until saturated.

127 **2.3 Experimental methods**

128 **2.3.1 Loading and freeze-thaw tests**

129 At 28 days, the compressive strength (f_c) of C30 and C50 were measured according to GB/T
130 50081-2002 [37], and the results were shown in Table 3. In loading test, hydraulic jack was
131 used to supply stress on specimen. Two different compression stress level, i.e. $0.3f_c$ and $0.5f_c$
132 were applied on. The exact pressure applied on concrete specimens can be read from a dial
133 attached to the hydraulic jack. Hydraulic pressure testing machine which was usually used by
134 normal compression test was also used in this study for comparison [38]. It was found that the
135 deviation of compressive strength results measured by hydraulic jack and hydraulic pressure
136 testing machine was less than 2 MPa. During the loading process, the whole loading devices
137 (including concrete specimens) were immersed in water for 4 days and then exposed to
138 freezing-thawing test according to GB/T 50082-2009 [39]. Every freeze-thaw cycle continued
139 for 3.5 h, with the highest temperature of 18 ± 2 °C and lowest temperature of -20 ± 2 °C. In total,
140 150 freezing-thawing cycles were conducted. The sequences of test flow were compiled in Fig.
141 1.

142 **2.3.2 Mass-loss testing**

143 The mass loss reflected the frost resistance of concrete. In this study, the mass loss of C30 and
144 C50 concrete without load was measured by electronic scale (with an accuracy of 0.05 g) during
145 freeze-thaw test. The average mass loss of three concrete specimens was used as the final value.

146 **2.3.3 Relative dynamic elasticity modulus characterization**

147 Frost damage could influence the pore structure of concrete which could be reflect by its
148 relative dynamic elasticity modulus (RDM). The machine used for RDM test in this
149 contribution is KON-NM-4B non-metal ultrasonic testing analyser (CX2009XJ0179, Koncrete,
150 China), which includes transmitting port (output high voltage pulse) and receiving port
151 (receiving ultrasonic waves through concrete). After freeze-thaw cycles, the change of cracks
152 and pore structure inside concrete affected the transportation of ultrasonic waves through
153 concrete, directly reflected in the transport velocity values (V_n). Relative dynamic modulus
154 (E_{rd}) was calculated by Eq. (1). According to ACTM C 666 [32, 40], concrete was damaged
155 once its RDM loss exceed the critical value (i.e. 60%).

$$E_{rd} = \frac{E_{dn}}{E_{d0}} = \frac{V_n^2}{V_0^2} \quad (1)$$

156 Where, E_{rd} = the relative dynamic modulus, %;

157 E_{dn} = the dynamic modulus of concrete after n freeze-thaw cycles, Hz;

158 E_{d0} = the dynamic modulus of concrete before freeze-thaw cycles, Hz;

159 V_n = the transport velocity values after n freeze-thaw cycles, m/s;

160 V_0 = the transport velocity values before freeze-thaw cycles, m/s;

161 **2.3.4 Capillary water absorption test and Chloride penetration test**

162 **2.3.4.1 Cutting**

163 After certain freezing-thawing cycles (0, 25, 50, 100 and 150 cycles), the concrete specimens
164 were unloaded and cut into four pieces. One cube concrete specimen were divided into two
165 sets; each set includes one inside piece and one outside piece. One set was used for capillary
166 water absorption test and the other one was used for chloride penetration test. Table 4 shows
167 the definition examples of different concrete specimens. Specimens were designate in the form
168 of “XX-CC-i/o” where XX representing applied compression stress level, CC representing
169 frost cycles, and i/o representing inside piece or outside piece of concrete specimen. After
170 cutting, all pieces were dried in oven at 60 °C for 24 h and then cooled to ambient temperature
171 for 12 h. This step could evaporate all free water inside of concrete to improve the accuracy of
172 the water absorption tests and chloride intrusion [41]. To ensure one-dimensional diffusion of
173 moisture, the other four sides of concrete piece that are perpendicular to the absorbent surface
174 were sealed with paraffin wax [42].

175 **2.3.4.2 Water absorption test**

176 When concrete was exposed to water, water could enter inside of materials through capillary
177 pressure. This phenomenon was related to many durability related issues, e.g. chloride

178 penetration, hence damage the concrete structure [38, 43, 44]. The water absorption of concrete
179 were measured by the time dependent amount of water that was absorbed by capillary pores in
180 concrete. The amount of capillary absorption water of concrete gradually decays with the
181 square root of absorption time, which could be described using the following equation [23, 43].

$$\Delta W = A\sqrt{t} \quad (2)$$

182 Where, A = the water absorption coefficient, $\text{g/m}^2 \cdot \text{h}^{0.5}$; t = the immersion time of specimens in
183 water or 3.5% NaCl solution, hour; t varies from 0 h, 0.5 h, 1 h, 2 h, 4 h, 8 h, 12 h, 24 h, 48 h,
184 72 h, 168 h, 336 h and 672 h.

185 Due to the effect of gravity, the mass of absorbed water could compensate with capillary
186 pressure with the increase of absorbed time. As shown in Fig. 4 and Fig. 5, the lines tend to
187 steady with the increase of time. This process could be described in an empirical exponential
188 function as shown in Eq. (3). The parameters a and b was determined by fitting Eq. (2) with
189 experimental data as shown in Fig. 4 and Fig. 5.

$$\Delta W = a[1 - \exp(-b\sqrt{t})] \quad (3)$$

190 The time-dependent coefficient ($A(t)$) of capillary water absorption was obtained by Eq. (4).

191 The initial coefficient of capillary water absorption A_i could be determined by Eq. (5) [23, 38].

$$A(t) = \frac{d\Delta W}{d\sqrt{t}} = a \times b \exp(-b\sqrt{t}) \quad (4)$$

$$A_i = a \times b \quad (5)$$

192 **2.3.4.3 Chloride Penetration tests**

193 **1) Preparation of concrete powder**

194 As mentioned in Section 2.2.3.1, one outside concrete piece and inside concrete piece were put
195 in contact with NaCl solution with a concentration of 3.5%. The experiment set-up is the same
196 as the water absorption test. After exposure to NaCl solution for certain age (7 days and 28
197 days), concrete were taken out of the container and grinded into powder layer by layer [45].
198 For the grinding procedure, the concrete block was first fixed on the grinding machine, and the
199 grinding head was adjusted to contact the surface of concrete and started to grind. The grinding
200 machine was shown in [45]. Each layer was milled with a thickness of 2 mm. In total, a depth
201 of 20 mm was ground for each concrete specimen. The obtained concrete powder was sieve
202 with a 0.63 mm sieve-mesh and dried in an oven at a temperature of 55 ± 5 °C for 2 hours.
203 After drying, concrete powder was put in in a desiccator to room temperature, and then sealed
204 for use.

205 **2) Determination of chloride ion content**

206 The chloride content of the obtained powder was determined according to GB11896-89 [46].
207 In this experiment, 2 grams of concrete powder was mixed with 50 ml distilled water (V_1) and
208 shake for 15-20 minutes. After mixing the suspension liquid was stand still for 24 hours and
209 filtered. Afterwards, 20 ml filtrate (V_2) was pipetted and put into an Erlenmeyer flask. 2 drops
210 of phenolphthalein was first added in the solution, then neutralized with dilute sulfuric acid
211 until the solution became colourless. Afterwards, 10 drops of potassium chromate reagent was

212 added in the flask, and titrated with standard silver nitrate solution (0.02 mol/L) to become red
213 colour and recorded the volume (V_3) consumed by silver nitrate.

214 The free chloride content was calculated as Eq. (6) [47, 48]:

$$P = \frac{C_{AgNO_3} V_3 \times 0.03545}{G \times \frac{V_2}{V_1}} \times 100\% \quad (6)$$

215 Where: P = the free chloride content in concrete;

216 G = the weight of concrete powder, 2 grams;

217 V_1 = the water used to dissolved concrete powder, 50 ml;

218 V_2 = the filtrate used for titration, 20 ml;

219 V_3 = the $AgNO_3$ used for titration.

220 **2.3.5 Mercury intrusion porosimetry test (MIP)**

221 The mercury intrusion porosimetry used in this study is Pore – master – 33. The measurement
222 was conducted in two stages: the first stage is the low pressure stage; the second stage is the
223 high pressure stage. The highest pressure can reach 33000 Psi (1 Psi = 6.895 kPa). Washburn
224 equation (Eq. (6)) was used to calculate the diameter of pores intruded by mercury at each
225 pressure step.

$$D = -4\gamma\cos\theta/P \quad (6)$$

226 Where D is the pore diameter, γ is the surface tension of mercury, θ is the contact angle
227 between mercury and AAF materials and P is the applied pressure. The surface tension used
228 here is 0.485 N/m, and the contact angle is 132° . According to Washburn equation, the pore
229 size ranging from 360 μm to 0.005 μm can be detected in this study.

230 The samples used for MIP test were damaged concrete pieces that was exposed to frost cycles
231 and applied load. First, concrete piece was broken by hammer with hand and coarse aggregate
232 were removed out from mortar. The mortar was then immediately immersed in ethanol to
233 terminate the hydration. Before test, samples were dried by oven and cooled to room
234 temperature.

235 **3. Results and discussion**

236 **3.1 Mechanical behaviour**

237 **3.1.1 The mass loss of concrete exposed to freeze-thaw cycles**

238 Fig. 2 shows the mass loss rate of C30 and C50 concrete during freeze-thaw cycles without
239 loading. For C30 concrete, there is a sharp mass-loss after 25 frost cycles which indicating the
240 initiation damage of concrete. C50 concrete showed much slower weight loss than C30
241 concrete during frost cycles. For example, when freeze-thaw cycles reached 150 times, the
242 mass loss rate of C50 was 0.59%, significantly lower than that of C30 concrete (4.49%). The
243 mass loss of concrete was mainly caused by the loss of mortar on the concrete surface [49].
244 C50 concrete had lower water/cement ratio and denser microstructure than C30 concrete.

245 Hence during freeze-thaw cycles, the saturated water in C50 concrete was lower than C30
246 concrete, resulting in less damage during frost cycles. Water/cement ratio showed importance
247 in frost resistance of ordinary Portland concrete [50].

248 **3.1.2 The loss of relative dynamic modulus (RDM) of concrete under compressive load** 249 **and freeze-thaw cycles**

250 Fig. 3 shows the change of RDMs of C30 and C50 concrete under different compression stress
251 ratio and frost cycles. It is obvious that the RDMs of C30 and C50 both decreased with
252 increasing frost cycles. It is interesting to find that concrete samples under 30%ultimate load
253 ($0.3f_c$) presented the smallest RDM loss than samples without loading ($0f_c$) and with 50%
254 ultimate load ($0.5f_c$). For example, the RDM loss of C30 concrete with $0.3f_c$ load was 7.9%,
255 compared to 39.4% and 43.1% for concrete C30 with $0f_c$ load and $0.5f_c$ load, respectively. The
256 same phenomenon was also found in C50 concrete. It means that the application of a certain
257 compressive load on concrete could increase its frost resistance. Compared to C30 concrete,
258 C50 concrete had less RDM loss after same freeze-thaw cycles, which means C50 concrete
259 performed better frost resistance than C30 concrete.

260 It is speculated that the loss process of RDM depended on the pore structure in concrete during
261 the freeze-thaw process. At low temperature (lower than 0°C), the volume of closed pore in
262 concrete expanded due to icing [51]. This expand force was counteracted by a certain
263 compressive load. Thus, when the compressive ratio was 0.3 ($0.3f_c$), concretes showed higher
264 frost resistance than concretes without loading. With the increase of loading (stress ratio is 0.5

265 in this study), the applied stress exceeded the expand force, secondary cracks were generated
266 [52-54]. As discussed in section 2.3.3, cracks inside concrete reduced the transport velocity
267 values, which leading to a higher RDM loss.

268 **3.2 Water absorption of concrete under coupling effect of compressive load and** 269 **freeze-thaw cycles**

270 Water absorption was regarded as a useful indicator to evaluate the damage of concrete under
271 coupling effect of compressive load and freeze-thaw cycles [41]. Fig. 4 shows the amount of
272 absorbed water of C30 concrete under coupling effect of load and freeze-thawing cycles. It was
273 found that the amount of absorbed water increased with the immersing time. For outside
274 concrete specimens, the amount of absorbed water of concrete under 30% ultimate load ($0.3f_c$)
275 shows lower water absorption content than that without load, while the concrete under 50%
276 ultimate load ($0.5f_c$) shows the highest. For inside concrete specimens, it is clear to see that the
277 concrete under $0.5f_c$ shows relatively higher water absorption amount, while concrete under
278 $0.3f_c$ shows similar water absorption amount in comparison with that without load.

279 As shown in Fig. 4, the black dashed line is the base line of samples without any damage from
280 frost and load. Compare spacing between the black dashed line with samples, we could find
281 that the increment of the amount of absorbed water of the samples under $0.3f_c$ is smaller than
282 other two samples. Particularly, when frost cycles increased from 25 to 50, there is
283 inconspicuous increase for samples under $0.3f_c$. It is different with the results that observed by
284 Zhang et al. [23], the amount of absorbed water increased with freeze-thaw cycles (0, 10, 50

285 and 100 cycles) if samples without applied load. This means that the service life prediction of
286 concrete structures becomes complex if applied mechanical load and environmental load.

287 It is known that water absorption content was closely related to the capillary pores in concrete.
288 A certain compressive stress could compact existing cracks in concrete and hinder the
289 generation of new cracks, resulting in a lower water absorption content. When the applied load
290 reached 50% ultimate load ($0.5f_c$), the excessive load induced new cracks in concrete and then
291 water absorption content increased. Bao and Wang [34] also found that cumulative water
292 content decreased when applied load increased from 0% to 19.81%, and then increased from
293 34.21% to 49.55%. We could find that, the influence of applied load on water absorption of
294 concrete showed less difference with or without freeze-thaw cycles.

295 The amount of absorbed water increased when frost cycles increased from 50 to 150. It
296 indicates that the frost damage generated more cracks in concrete with the increase of freeze-
297 thaw cycles. The new cracks provided more penetration path for water into concrete.

298 The amount of absorbed water of inside concrete specimen was less than that of the outside
299 specimens. It means that the damage caused by freeze-thaw cycles initiated from the outside,
300 then developed to the inside part [23]. It is reported that the freeze-thaw damage on concrete
301 included two aspects [6]: first is the peeling off surface mortar and then generation of internal
302 cracks. In this study, it is found that the internal damage happened after 50 freeze-thaw cycles,
303 before which the water absorption content was similar to inside samples (Fig. 4).

304 Fig. 5 shows the amount of absorbed water of C50 concrete under the coupling effect of load
305 and freeze-thaw cycles. In general, the amount of absorbed water of C50 exhibited similar trend
306 as C30, while the water absorption content of C50 was about 5 times smaller than that of C30,
307 both before and after the freeze-thaw cycles. It means that C50 concrete have a better water
308 resistance than C30 concrete under the coupling effect of load and frost cycles.

309 It is interesting to note that the water absorption content of C50 concrete under 30% ultimate
310 load ($0.3f_c$) showed close trend to that without loading. Samples under 50% ultimate load ($0.5f_c$)
311 showed a little higher water absorption content. Compared with C30 concrete, samples under
312 50% ultimate load ($0.5f_c$) showed a significant increase than that without loading. It means that
313 the applied stress had less influence on low water/cement ratio concrete (i.e. C50, $w/c=0.35$)
314 than high water/cement ratio concrete (i.e. C30, $w/c=0.53$).

315 Fig. 6 summarized the initial water absorption coefficient (A_i) of C30 and C50 as a function of
316 freeze-thaw cycles. It is clear that A_i exhibits an upward trend with the increase of freeze-thaw
317 cycles. For C30 concrete, after 50 freeze-thaw cycles, the A_i increased sharply. It means that
318 new cracks generated in concrete after 50 freeze-thaw cycles. For C50 concrete, the A_i was
319 much smaller than C30 concrete. The coupling effect of compressive load and freeze-thaw
320 cycles was more serious on C30 concrete than on C50 concrete [50].

321 **3.3 Chloride penetration of concrete under compressive load and freeze-thaw**
322 **cycles**

323 Fig. 7 and Fig. 8 show the chloride ion content of C30 concrete after 7d and 28 d chloride
324 penetration, respectively. The chloride ion content described with increasing depth. This is
325 because that chloride ions penetrated into concrete surface by capillary suction and then
326 diffused into deeper zones [38].

327 From Fig. 7, it is obvious that samples with $0.3f_c$ showed the least chloride ion content and
328 samples with $0.5f_c$ showed the highest. It means that $0.3f_c$ could help hinder the penetration of
329 chloride ion while $0.5f_c$ accelerate the penetration. This is because that a certain compression
330 stress level compact the pore structure of concrete. The penetration of chloride ion into concrete
331 was hindered [35, 38, 55, 56]. The penetration depth and the amount of chloride ion
332 significantly increased with the increase of freeze-thaw cycles. Frost action before 50 freeze-
333 thaw cycles did not apparently influence the penetration of chloride ion, which similar to the
334 water absorption [57]. Compared with the results found by Zhang et al. [23], the amount of
335 chloride penetration increased obviously with the increase of freeze-thaw cycles without load.
336 The chloride penetration became complex and unstable if applied load. The results suggested
337 that a certain compression load was encouraged for concrete structure in cold coast area [26].
338 It suggested that a certain of compressive stress should be concerned into the durability design
339 of reinforcement concrete structure.

340 It is also found that the chloride ion content of inside concrete specimen was less than that of
341 the outside part. This is because that the peeling off of the surface of outside part which exposed
342 to freeze-thaw solution provided new penetration pathway for chloride ion into concrete [23,
343 58]. It is suggested that a protective treatment on the surface of concrete could develop to
344 enhance the durability of structure.

345 From the comparison of Fig. 7 and Fig. 8, it is obvious that the penetration depth and amount
346 of chloride ion increased significantly after 28 d chloride penetration. For example, the chloride
347 ion content of 7 d at 20 mm depth was less than 0.05% of concrete while chloride ion content
348 of 28 d still kept down trend after 20 mm. According to Wittmann et al. [59], raw material and
349 tap water could carry around 0.05% chloride into concrete. This means that in this study
350 chloride ion penetrated into deeper depth than 20mm after 28d penetration [23, 38].

351 Fig. 9 and Fig. 10 showed the chloride ion content of C50 concrete after 7 d and 28 d chloride
352 penetration. Similar change trend of chloride ion content occurred between C30 and C50 refer
353 to the influence of coupling effect of freeze-thaw and stress level. It is noted that the chloride
354 ion content of C50 tended to smooth at 10 mm while C30 concrete kept downward trend after
355 20 mm. Chloride penetration rate of C50 was much lower than C30. This indicated that C50
356 performs better chloride resistance than C30. This observation can be explained
357 phenomenologically by the difference of water/ratio. Lower w/c ration could synthesis more
358 impact concrete and shows higher damage resistance to coupling effect [23, 50]. Wang et al.

359 [48] also found that with the increase of the compressive stress (from 22% to 51%), the chloride
360 concentration at a given depth was decreased, especially for the concretes C30 (w/c = 0.50) .

361 **3.4 Pore size distribution**

362 Fig. 11 showed the pore size distribution of C30 concrete under different compressive stress
363 ratio after 50 freeze-thaw cycles. For all the samples, generally one peak (in the range of 10-
364 1000 nm) was shown in Fig.15, representing the capillary pores of C30. Due to “ink-bottle”
365 effect and contact angle, the real pore diameter of capillary pores in C30 may be tens of times
366 larger than the results in MIP. However, the comparison of equal treatment samples can still
367 provide some valuable information on the pore structure.

368 As suggested by Mehta [19] and Chen [20], capillary effect decreased firstly and then increased
369 with the pore size decreased from 10000nm to 100nm. After 50 freeze-thaw cycles, the peak
370 corresponding to the capillary pore in $0.5f_c$ was the highest, while the peak of $0f_c$ (without
371 loading) and $0.3f_c$ was lower, indicating that concrete samples under $0.5f_c$ was the highest water
372 absorption and chloride induction. Samples without load or freeze-thaw cycles showed the
373 smallest peak value and relatively lower amount of absorbed water and chloride ions.

374 From comparison between undamaged samples with damaged samples, it proves that frost
375 action lead to a percentage increment of coarse pores, resulting in an increment of absorbed
376 water and chloride. At the meantime, 50% ultimate compressive stress encouraged the frost
377 damage while 30% ultimate compressive stress could reduce.

378 From above results, we could confirm that stress played a relatively important role in the water
379 absorption and chloride penetration of concrete under coupling effect of load and freeze-thaw.
380 It means that a certain stress level (30% ultimate strength in this study) could improve the
381 resistance of concrete to water and aggressive solution during freeze-thaw cycles. The above
382 result provided key information regarding to the service life design or durability design of
383 concrete structure in cold coast area.

384 **4. Conclusions**

385 From the result presented in this paper, the following conclusions can be drawn:

- 386 1. The amount of absorbed water and chloride ion increased slightly before 50 freeze-
387 thaw cycles and sharply after 100 and 150 cycles. Freeze thaw shifted the pore size
388 distribution towards microporous and generate new cracks, which provided new
389 penetration path for water and chloride ion into concrete.
- 390 2. C50 concrete showed better penetration resistance to water and chloride ion than C30
391 concrete. The effect of applied load had much less impact on the Cl penetration than
392 C30 concrete. Water/cement ratio is the decisive factor on the durability performance
393 of concrete. The applied load ($0.3f_c$) had inconspicuous effect on C50 concrete.
- 394 3. For C30 concrete, a certain stress ($0.3f_c$) could help relieve the damage caused by frost
395 and Cl ingression, while excessive load ($0.5f_c$) could aggravate damage. The influence
396 of load should be concerned into the durability design of reinforcement concrete
397 structure exposed to marine environment.

398 4. Under coupling effect of load and freeze-thaw, applied load could cause significant
399 change to the freeze-thaw resistance of concrete; however, the unfluence of load on the
400 durability of concrete is slightly changed by freeze-thaw.

401 **Acknowledgements**

402 Financial support of ongoing projects by Natural Science Foundation of China (51420105015,
403 U1706222, 51778309), 973 Program (2015CB655100), and Natural Science Foundation of
404 Shandong Province (ZR201709210171, ZR2017ZC0737) is greatly acknowledged.

405 **References**

- 406 1. Aïtcin, P.-C., Cements of yesterday and today: Concrete of tomorrow. *Cement and Concrete*
407 *Research*, 2000. **30**(9): p. 1349-1359.
- 408 2. Powers, T.C. A working hypothesis for further studies of frost resistance of concrete. in *Journal*
409 *Proceedings*. 1945.
- 410 3. Wang, P.G., et al. Influence of Sustained Load on Durability and Service Life of Reinforced
411 *Concrete Structures*. in *Key Engineering Materials*. 2016. Trans Tech Publ.
- 412 4. Glasser, F.P., J. Marchand, and E. Samson, Durability of concrete—degradation phenomena
413 involving detrimental chemical reactions. *Cement and Concrete Research*, 2008. **38**(2): p. 226-
414 246.
- 415 5. Pigeon, M. and R. Pleau, Durability of concrete in cold climates. 2010: CRC Press.
- 416 6. Yang, Z., W.J. Weiss, and J. Olek, Water Transport in Concrete Damaged by Tensile Loading
417 and Freeze-Thaw Cycling. *Journal of Materials in Civil Engineering*, 2006. **18**(3): p.
418 424-434.
- 419 7. Wilson, M., M. Carter, and W. Hoff, British Standard and RILEM water absorption tests: A
420 critical evaluation. *Materials and Structures*, 1999. **32**(8): p. 571-578.
- 421 8. Dullien, F.A., Porous media: fluid transport and pore structure. 2012: Academic press.
- 422 9. Boddy, A., et al., An overview and sensitivity study of a multimechanistic chloride transport
423 model. *Cement and concrete research*, 1999. **29**(6): p. 827-837.
- 424 10. Yong, R.N., A.-M.O. Mohamed, and B.P. Warkentin, Principles of contaminant transport in
425 soils. 1992: Elsevier Science Publishers.
- 426 11. Gutiérrez-Padilla, M.G.D., et al., Biogenic sulfuric acid attack on different types of
427 commercially produced concrete sewer pipes. *Cement and Concrete Research*, 2010. **40**(2): p.
428 293-301.
- 429 12. Wang, L. and S. Li, Capillary absorption of concrete after mechanical loading. *Magazine of*
430 *Concrete Research*, 2014. **66**(8): p. 420-431.
- 431 13. Martys, N.S. and C.F. Ferraris, Capillary transport in mortars and concrete. *Cement and*
432 *Concrete Research*, 1997. **27**(5): p. 747-760.
- 433 14. Dehghanpoor Abyaneh, S., H.S. Wong, and N.R. Buenfeld, Computational investigation of
434 capillary absorption in concrete using a three-dimensional mesoscale approach. *Computational*
435 *Materials Science*, 2014. **87**: p. 54-64.
- 436 15. Mors, R.R.M.M.t.n.b.c. and H.H.M.J.t.n. Jonkers, Effect on Concrete Surface Water
437 Absorption upon Addition of Lactate Derived Agent. *Coatings* (2079-6412), 2017. **7**(4): p. 1-
438 10.
- 439 16. Soroushian, P., H. Chowdhury, and T. Ghebrab, Evaluation of Water-Repelling Additives for
440 Use in Concrete-Based Sanitary Sewer Infrastructure. *Journal of Infrastructure Systems*, 2009.
441 **15**(2): p. 106-110.
- 442 17. Şahmaran, M. and V.C. Li, Influence of microcracking on water absorption and sorptivity of
443 ECC. *Materials and Structures*, 2009. **42**(5): p. 593-603.
- 444 18. Wu, L., et al., Autogenous shrinkage of high performance concrete: A review. *Construction and*
445 *Building Materials*, 2017. **149**: p. 62-75.

- 446 19. Mehta, P.K., Studies on blended Portland cements containing Santorin earth. *Cement and*
447 *Concrete Research*, 1981. **11**(4): p. 507-518.
- 448 20. Chen, L.W., Yongping; Yin, Xinshen; Zhang, Dan, Effect of aperture size on impermeability
449 of concrete. *Journal of The Chinese Ceramic Society*, 2005. **33**(4): p. 500-505.
- 450 21. Zhang, S.P. and L. Zong, Evaluation of Relationship between Water Absorption and Durability
451 of Concrete Materials. *Advances in Materials Science & Engineering*, 2014: p. 1-8.
- 452 22. Zuquan, J., et al., Chloride ions transportation behavior and binding capacity of concrete
453 exposed to different marine corrosion zones. *Construction and Building Materials*, 2018. **177**:
454 p. 170-183.
- 455 23. Zhang, P., et al., Influence of freeze-thaw cycles on capillary absorption and chloride
456 penetration into concrete. *Cement and Concrete Research*, 2017. **100**: p. 60-67.
- 457 24. Cui, F.-k., et al., Mechanical and Failure Criteria of Air-Entrained Concrete under Triaxial
458 Compression Load after Rapid Freeze-Thaw Cycles. *Advances in Materials Science &*
459 *Engineering*, 2017: p. 1-8.
- 460 25. Zhang, P., et al., Effect of Air Entrainment on the Mechanical Properties, Chloride Migration,
461 and Microstructure of Ordinary Concrete and Fly Ash Concrete. *Journal of Materials in Civil*
462 *Engineering*, 2018. **30**(10): p. 04018265.
- 463 26. Zhang, P., et al., Steel reinforcement corrosion in concrete under combined actions: The role of
464 freeze-thaw cycles, chloride ingress, and surface impregnation. *Construction and Building*
465 *Materials*, 2017. **148**: p. 113-121.
- 466 27. Tennakoon, C., et al., Chloride ingress and steel corrosion in geopolymer concrete based on
467 long term tests. *Materials & Design*, 2017. **116**: p. 287-299.
- 468 28. Zhang, P., et al., Application of neutron imaging to investigate fundamental aspects of
469 durability of cement-based materials: A review. *Cement and Concrete Research*, 2018. **108**: p.
470 152-166.
- 471 29. Costa, A. and J. Appleton, Chloride penetration into concrete in marine environment—Part I:
472 Main parameters affecting chloride penetration. *Materials and Structures*, 1999. **32**(4): p. 252.
- 473 30. Collepardi, M., A. Marcialis, and R. Turriziani, Penetration of chloride ions into cement pastes
474 and concretes. *Journal of the American Ceramic Society*, 1972. **55**(10): p. 534-535.
- 475 31. Cai, H. and X. Liu, Freeze-thaw durability of concrete: ice formation process in pores. *Cement*
476 *and Concrete Research*, 1998. **28**(9): p. 1281-1287.
- 477 32. Molero, M., et al., Evaluation of freeze–thaw damage in concrete by ultrasonic imaging. *NDT*
478 *& E International*, 2012. **52**: p. 86-94.
- 479 33. Sun, J. and L. Lu, Coupled effect of axially distributed load and carbonization on permeability
480 of concrete. *Construction and Building Materials*, 2015. **79**: p. 9-13.
- 481 34. Bao, J. and L. Wang, Combined effect of water and sustained compressive loading on chloride
482 penetration into concrete. *Construction and Building Materials*, 2017. **156**: p. 708-718.
- 483 35. Sun, W., et al., Damage and damage resistance of high strength concrete under the action of
484 load and freeze-thaw cycles. *Cement and Concrete Research*, 1999. **29**(9): p. 1519-1523.
- 485 36. Tsvivilis, S., et al., A study on the parameters affecting the properties of Portland limestone
486 cements. *Cement and Concrete Composites*, 1999. **21**(2): p. 107-116.

- 487 37. Standard, C., GB/T, 50081-2002 Method for testing mechanical properties of normal concrete.
488 Beijing, China, 2002.
- 489 38. Lu, W., et al., Influence of an applied compressive load on capillary absorption of concrete:
490 observation of anisotropy. *Restoration of Buildings and Monuments*, 2014. **20**(2): p. 131-136.
- 491 39. Standard, C.I., Testing methods for long-term and long-lasting performance of ordinary
492 concrete, Construction Industry Publications;GB/T 50082-2009. 2009, Standard Press of China:
493 Beijing, China.
- 494 40. Pigeon, M., R. Pleau, and P.-C. Aitcin, Freeze-thaw durability of concrete with and without
495 silica fume in ASTM C 666 (Procedure A) test method: internal cracking versus scaling.
496 *Cement, concrete and aggregates*, 1986. **8**(2): p. 76-85.
- 497 41. Wittmann, F., et al. Service life of reinforced concrete structures under combined mechanical
498 and environmental loads. in *2nd International Symposium on Service Life Design for*
499 *Infrastructures*. 2010. RILEM Publications SARL.
- 500 42. Hall, C., Water movement in porous building materials—I. Unsaturated flow theory and its
501 applications. *Building and Environment*, 1977. **12**(2): p. 117-125.
- 502 43. Litvan, G.G., Phase transitions of adsorbates. V. Aqueous sodium chloride solutions adsorbed
503 of porous silica glass. *Journal of Colloid and Interface Science*, 1973. **45**(1): p. 154-169.
- 504 44. Castro, J., D. Bentz, and J. Weiss, Effect of sample conditioning on the water absorption of
505 concrete. *Cement and Concrete Composites*, 2011. **33**(8): p. 805-813.
- 506 45. Hong, F. and Z. Tiejun, DRB-H1 Fourth Generation Concrete Grinding Machine, in Patent,
507 China. 2004.
- 508 46. Zhang, Q., et al., Diffusion kinetics of sodium chloride in Grass carp muscle and its diffusion
509 anisotropy. *Journal of Food Engineering*, 2011. **107**(3): p. 311-318.
- 510 47. LI, S. and W. SUN, Review on deterioration of concrete subjected to coupling effect of fatigue
511 load, carbonation and chlorides. *Journal of The Chinese Ceramic Society*, 2013. **41**(11): p.
512 1459-1464.
- 513 48. Wang, H., et al., Effect of External Loads on Chloride Transport in Concrete. *Journal of*
514 *Materials in Civil Engineering*, 2011. **23**(7): p. 1043-1049.
- 515 49. Shang, H.-s. and Y.-p. Song, Behavior of air-entrained concrete under the compression with
516 constant confined stress after freeze–thaw cycles. *Cement and Concrete Composites*, 2008.
517 **30**(9): p. 854-860.
- 518 50. Wittmann, F., P. Zhang, and T. Zhao, Influence of combined environmental loads on durability
519 of reinforced concrete structures. *Restoration of Buildings and Monuments*, 2006. **12**(4): p.
520 349-362.
- 521 51. Zhang, P., et al., Self-healing behaviour of multiple microcracks of strain hardening
522 cementitious composites (SHCC). *Construction and Building Materials*, 2018. **169**: p. 705-715.
- 523 52. Dry, C., Three designs for the internal release of sealants, adhesives, and waterproofing
524 chemicals into concrete to reduce permeability. *Cement and Concrete Research*, 2000. **30**(12):
525 p. 1969-1977.
- 526 53. Qi, C., J. Weiss, and J. Olek, Characterization of plastic shrinkage cracking in fiber reinforced
527 concrete using image analysis and a modified Weibull function. *Materials and Structures*, 2003.
528 **36**(6): p. 386-395.

- 529 54. Matallah, M., C. La Borderie, and O. Maurel, A practical method to estimate crack openings in
530 concrete structures. *International Journal for Numerical and Analytical Methods in*
531 *Geomechanics*, 2010. **34**(15): p. 1615-1633.
- 532 55. Samaha, H.R. and K.C. Hover, Influence of microcracking on the mass transport properties of
533 concrete. *Materials Journal*, 1992. **89**(4): p. 416-424.
- 534 56. Wang, K., et al., Permeability study of cracked concrete. *Cement and concrete research*, 1997.
535 **27**(3): p. 381-393.
- 536 57. Jiang, W.-q., et al., A numerical study on chloride diffusion in freeze-thaw affected concrete.
537 *Construction and Building Materials*, 2018. **179**: p. 553-565.
- 538 58. Osio-Norgaard, J., J.P. Gevaudan, and W.V. Srubar, A review of chloride transport in alkali-
539 activated cement paste, mortar, and concrete. *Construction and Building Materials*, 2018. **186**:
540 p. 191-206.
- 541 59. Wittmann, F.H., et al. Influence of an imposed tensile stress and subsequent self-healing on
542 capillary absorption and chloride penetration into HPFRCC. in *High Performance Fiber*
543 *Reinforced Cement Composites*. Stuttgart: International RILEM Workshop. 2015.

545 Table 1 Chemical compositions of Portland cement used in this study

Raw materials	Components (mass% as oxide)										
	CaO	SiO ₂	Al ₂ O ₃	MgO	SO ₃	Fe ₂ O ₃	K ₂ O	TiO ₂	MnO	Na ₂ O	P ₂ O ₅
P.I. 52.5	57.27	20.60	7.17	4.70	4.43	3.85	0.77	0.40	0.35	0.17	0.13

546

547

548 Table 2 Mix composition of concrete

Concrete	Water/Cement	Cement (kg/m ³)	Sand (kg/m ³)	Aggregate (kg/m ³)	Water (kg/m ³)	Superplasticizer
C30	0.53	375	750	1125	200	/
C50	0.35	450	675	1125	156.1	2.0%

549

550 Table 3 Result of ultimate compression test

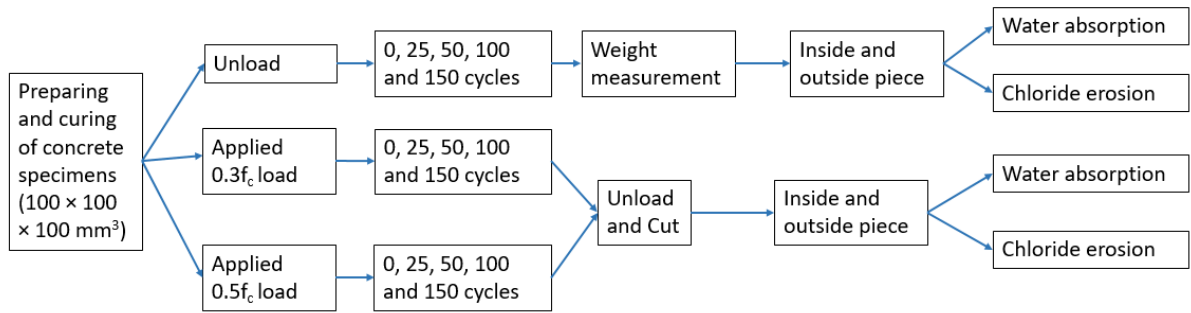
Concrete	Slump (mm)	Air content (%)	Bulk density (kg/m ³)	f_c (MPa)	$0.3f_c$ (MPa)	$0.5f_c$ (MPa)
C30	50	3.7	2414	38.47	12.2	20.3
C50	60	2.4	2470	54.95	17.4	28.9

551 f_c , the ultimate compressive strength after 28d curing, MPa

552

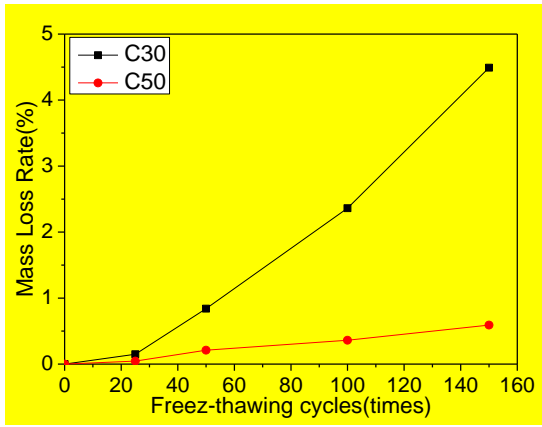
553 Table 4 Definition of different specimens

Specimen	Compressive stress f_c	Freezing-thawing cycles /cycle	Part
0-0-i	$0f_c$	0	Inside
0-0-o	$0f_c$	0	Outside
0-25-i	$0f_c$	25	Inside
0-25-o	$0f_c$	25	Outside
30-25-i	$0.3f_c$	25	Inside
30-25-o	$0.3f_c$	25	Outside
50-50-i	$0.5f_c$	50	Inside
50-50-o	$0.5f_c$	50	Outside



555

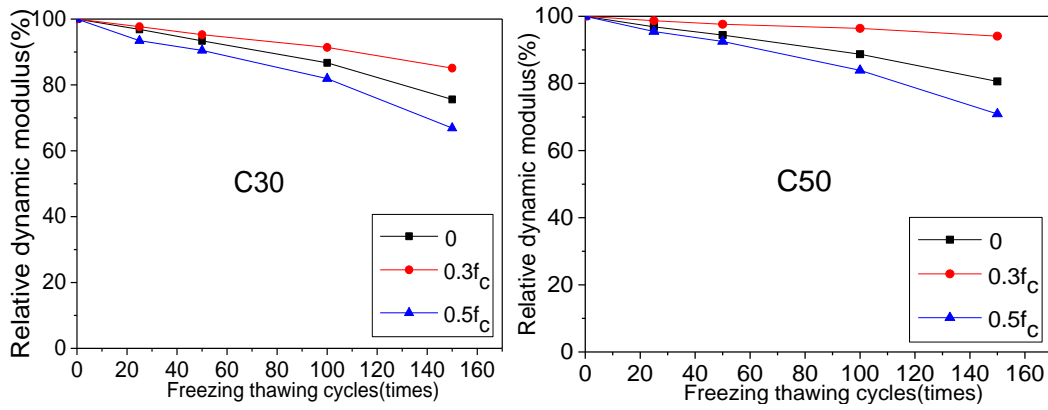
556 Fig. 1. Sequence of test flow



557

558 Fig. 2. The mass loss of concrete

559



560

561 **Fig. 3. The relative dynamic modulus (RDM) of C30 and C50 with the coupling effect of**
 562 **frost cycles and load**

563

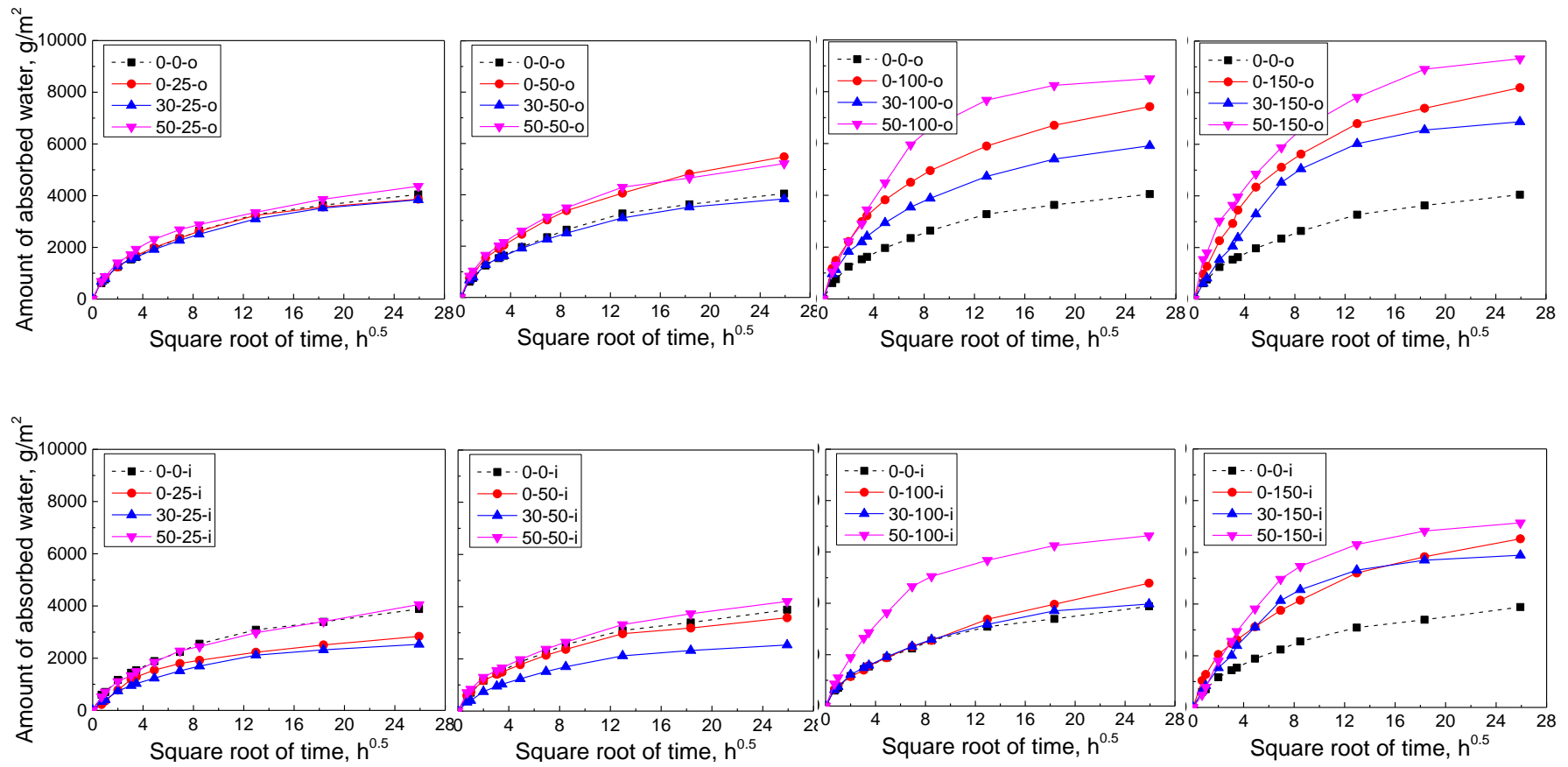


Fig. 4. Amount of absorbed water of C30 with the coupling effect of frost cycles and load

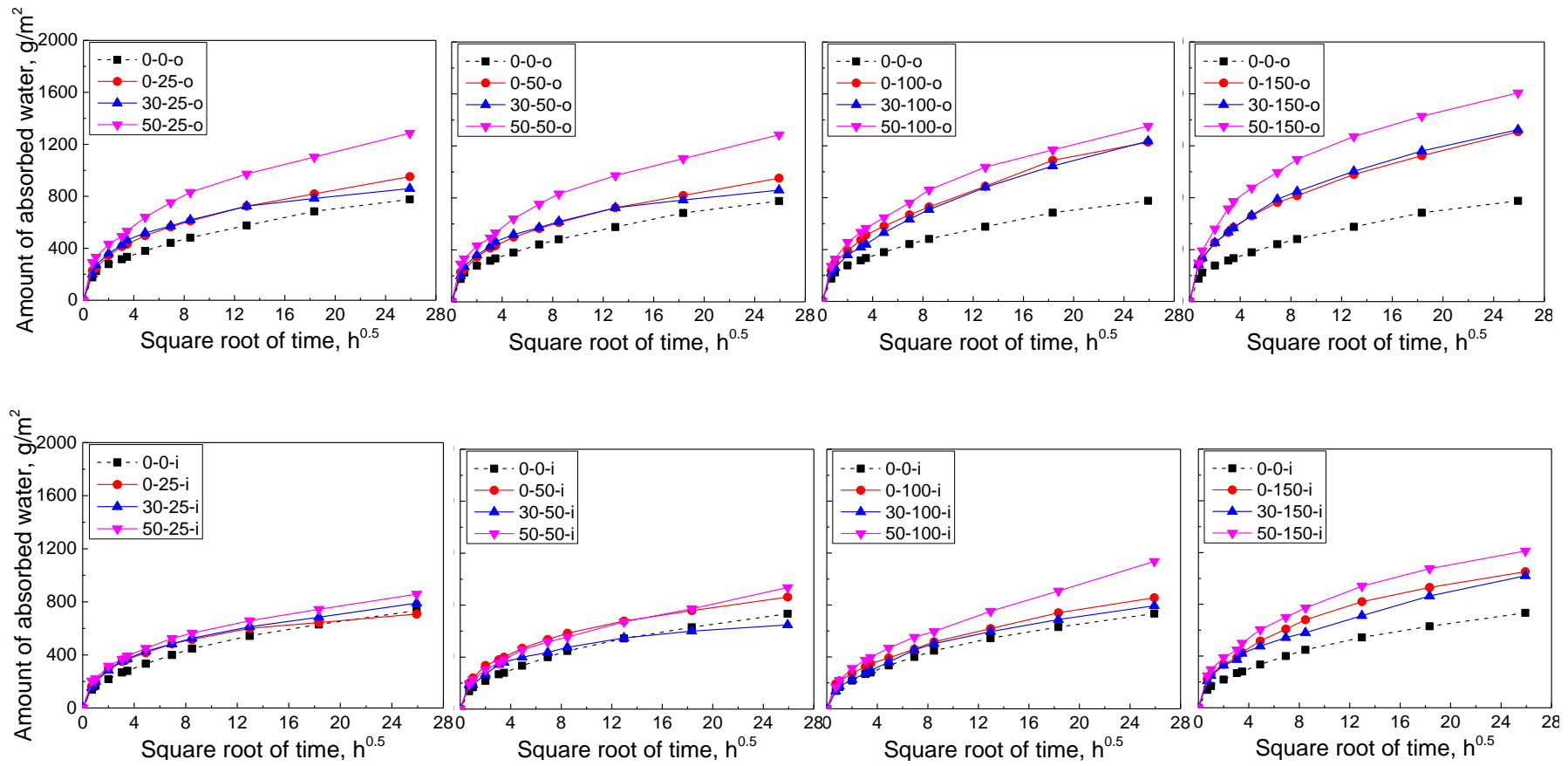


Fig. 5. Amount of absorbed water of C50 with the coupling effect of frost cycles and load

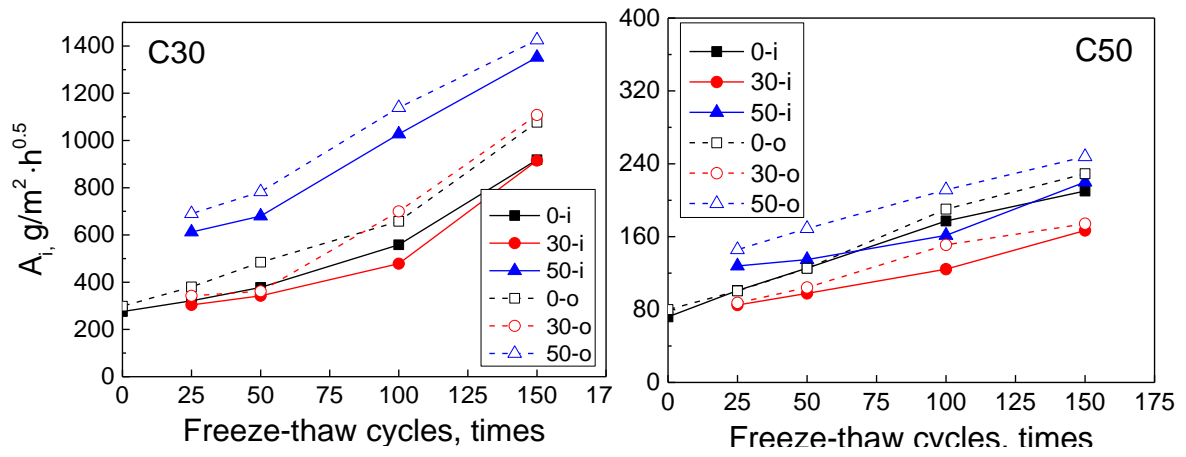


Fig. 6. Initial water absorption coefficient of C30 and C50 as function of freeze-thaw cycles

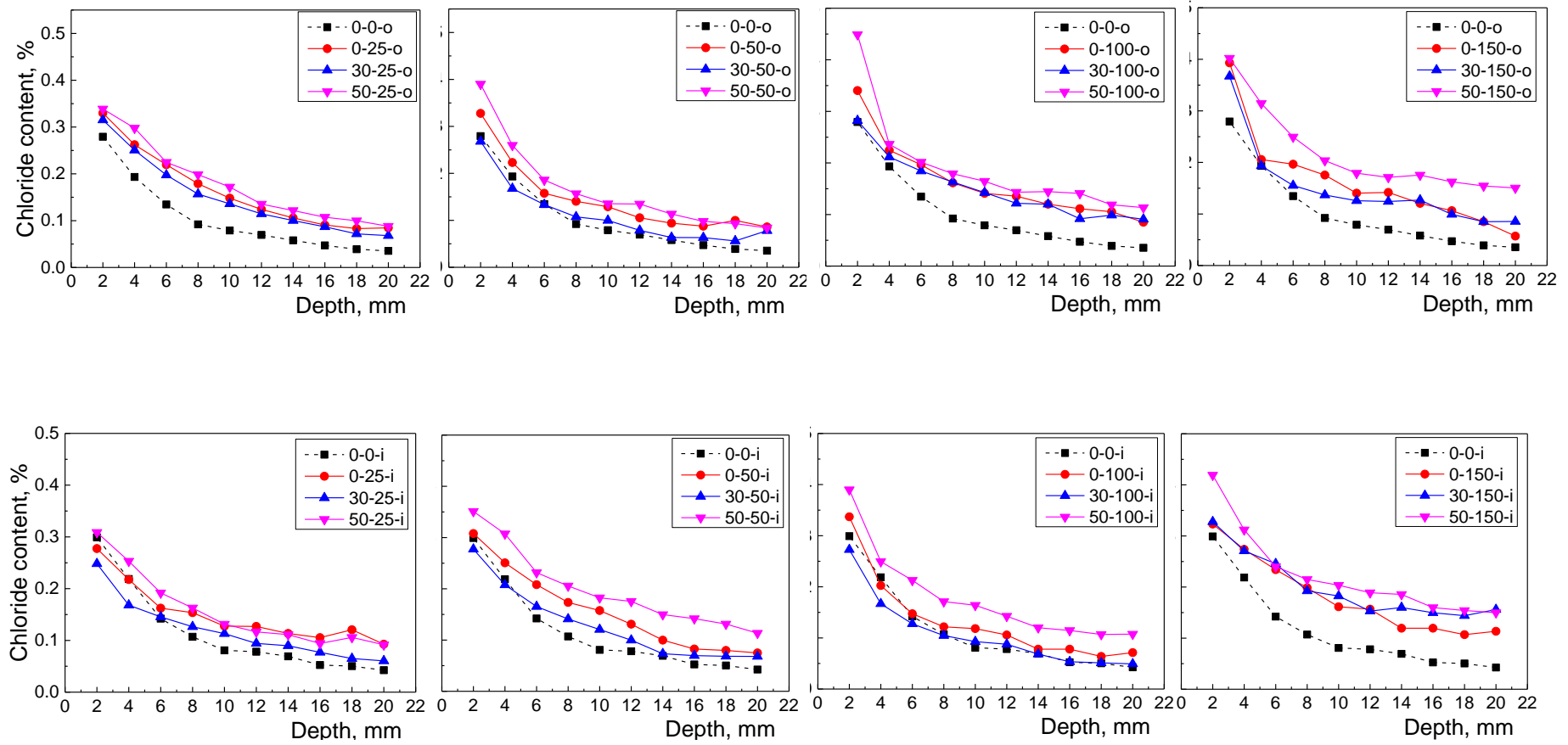
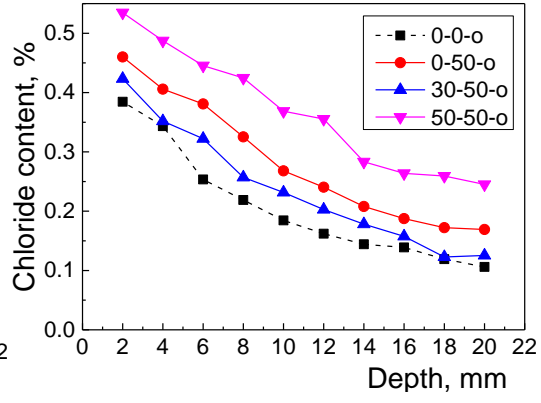
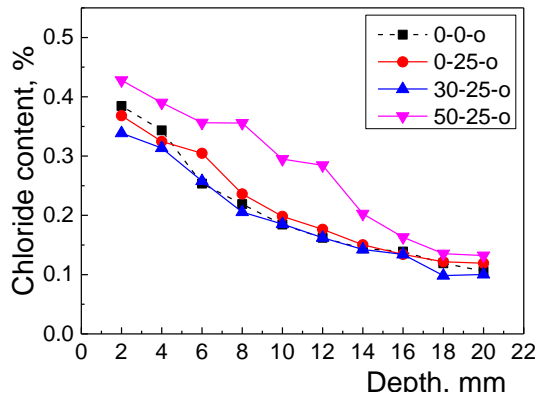
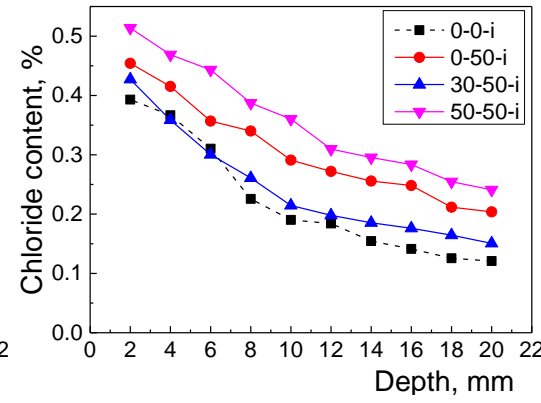
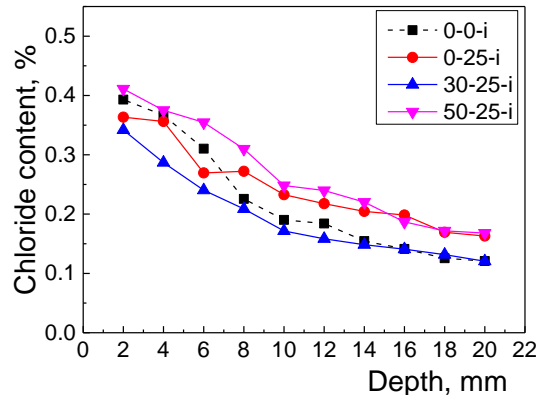


Fig. 7. Chloride ion content of C30 concrete after 7d chloride penetration

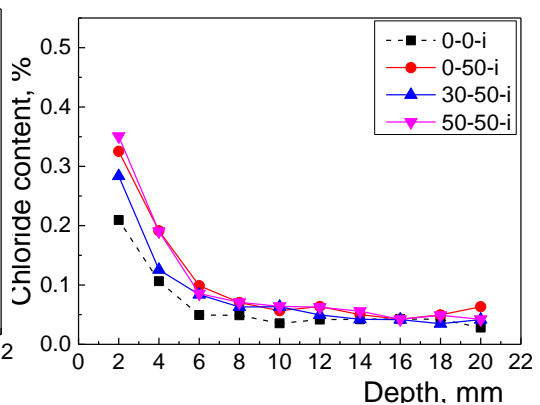
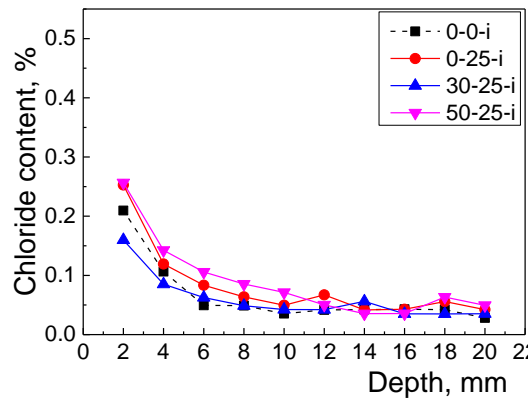
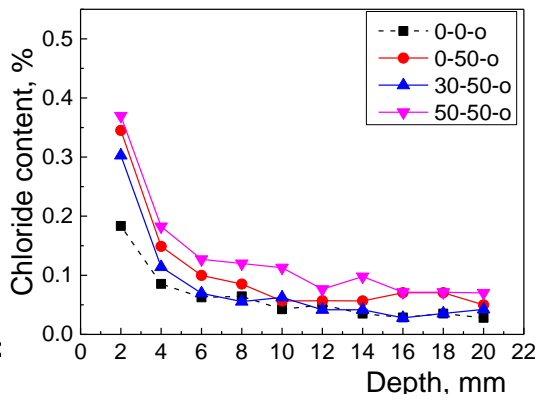
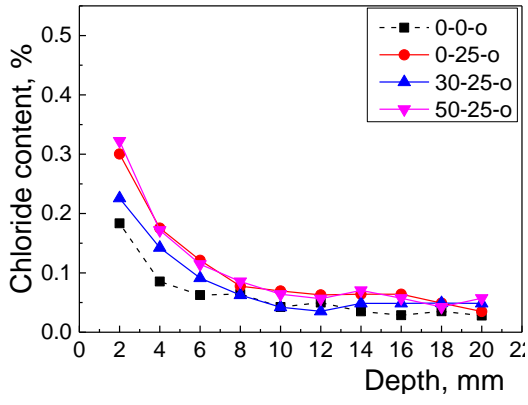


1



2

3 Fig. 8. Chloride ion content of C30 concrete after 28d chloride penetration

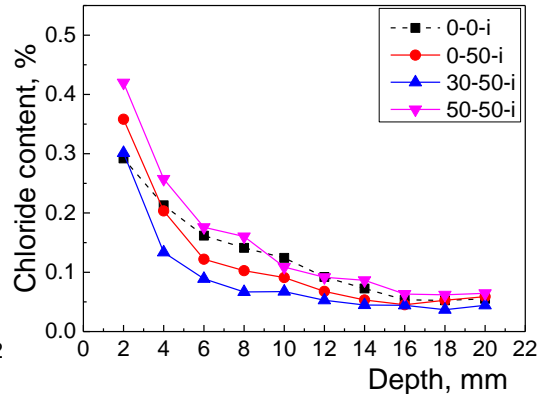
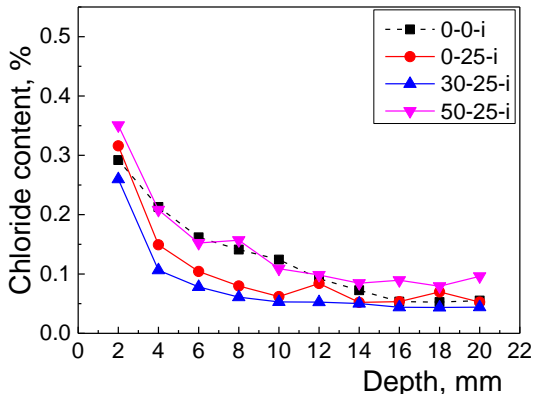
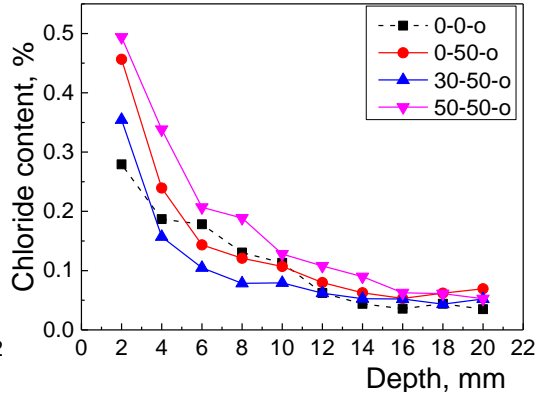
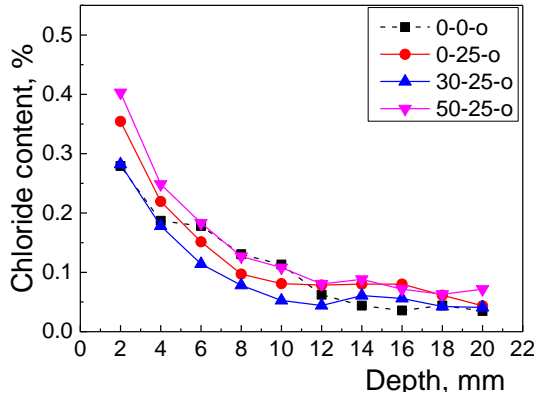


4

5

6 Fig. 9. Chloride ion content of C50 concrete after 7d chloride penetration

7

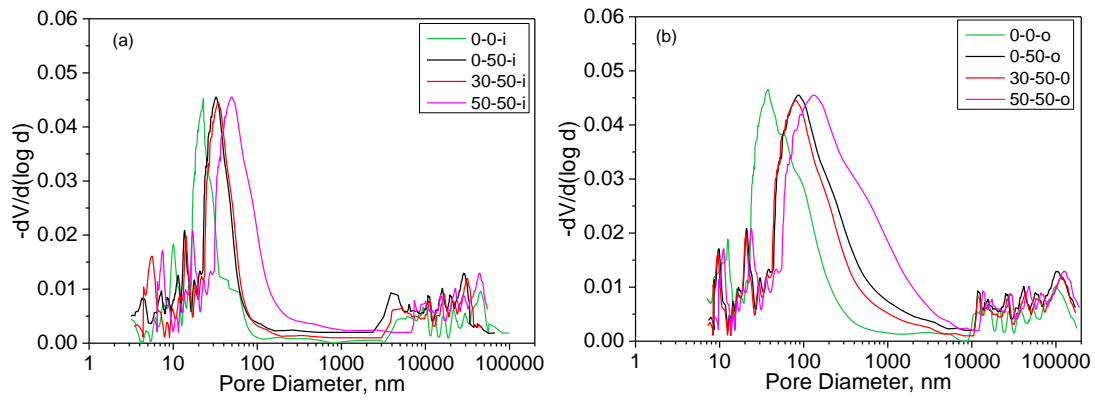


8

9

10 Fig. 10. Chloride ion content of C50 concrete after 28d chloride penetration

11



12

13 Fig. 11. Pore size distribution of C30 concrete under compiling effect